Review

Automatic Alignment for the first science run of the Virgo interferometer

F. Acernese [g,i], M. Alshourbagy [o,p], F. Antonucci [r], S. Aoudia [j], K.G. Arun [k], P. Astone [r], G. Ballardin [b], F. Barone [g,i], M. Barsuglia [z], Th.S. Bauer [t], S. Bigotta [o,p], S. Birindelli [j], M.A. Bizouard [k], C. Boccara [l], F. Bondu [j], L. Bonelli [o,p], L. Bosi [m], S. Braccini [o], C. Bradaschia [o], A. Brillet [j], V. Brisson [k], H.J. Bulten [t,u], D. Buskulic [a], G. Cagnoli [c], E. Calloni [g,h], E. Campagna [c,e], B. Canuel [b], F. Carbognani [b], L. Carbone [m], F. Cavalier [k], R. Cavalieri [b], G. Cella [o], E. Cesarini [c,d], E. Chassande-Mottin [z], S. Chatterji [r], F. Cleva [j], E. Coccia [v,w], J. Colas [b], M. Colombini [s], C. Corda [o,p], A. Corsi [r], J.-P. Coulon [j], E. Cuoco [b], S. D'Antonio [v], A. Dari [m,n], V. Dattilo [b], M. Davier [k], R. De Rosa [g,h], M. Del Prete [o,q], L. Di Fiore [g], A. Di Lieto [o,p], M. Di Paolo Emilio [v,y], A. Di Virgilio [o], V. Fafone [v,w], I. Ferrante [o,p], F. Fidecaro [o,p], I. Fiori [b], R. Flaminio [f], J.-D. Fournier [j], S. Frasca [r,s], F. Frasconi [o], L. Gammaitoni [m,n], F. Garufi [g,h], E. Genin [b], A. Gennai [o], A. Giazotto [o], M. Granata [z], V. Granata [a], C. Greverie [j], G. Guidi [c,e], H. Heitmann [j], P. Hello [k], S. Hild [aa], D. Huet [b], P. La Penna [b], M. Laval [j], N. Leroy [k], N. Letendre [a], M. Lorenzini [c], V. Loriette [l], G. Losurdo [c], J.-M. Mackowski [f], E. Majorana [r], C.N. Man [j], M. Mantovani [b,*], F. Marchesoni [m], F. Marion [a], J. Marque [b], F. Martelli [c,e], A. Masserot [a], F. Menzinger [b], C. Michel [f], L. Milano [g,h], Y. Minenkov [v], M. Mohan [b], J. Moreau [l], N. Morgado [f], S. Mosca [g,h], B. Mours [a], I. Neri [m,n], F. Nocera [b], G. Pagliaroli [v,w], C. Palomba [r], F. Paoletti [b,o], S. Pardi [g,h], A. Pasqualetti [b], R. Passaquieti [o,p], D. Passuello [o], G. Persichetti [g,h], F. Piergiovanni [c,e], L. Pinard [f], R. Poggiani [o,p], M. Punturo [m], P. Puppo [r], O. Rabaste [z], P. Rapagnani [r,t], T. Regimbau [j], F. Ricci [r,s], A. Rocchi [v], L. Rolland [a], R. Romano [g,i], P. Ruggi [b], B. Sassolas [f], D. Sentenac [b], B.L. Swinkels [b], R. Terenzi [v,x], A. Toncelli [o,p], M. Tonelli [o,p], E. Tournefier [a], F. Travasso [m,n], J. Trummer [a], G. Vajente [o,p], J.F.J. van den Brand [t,u], S. van der Putten [t], D. Verkindt [a], F. Vetrano [c,e], A. Viceré [c,e], J.-Y. Vinet [j], H. Vocca [m], M. Was [k], M. Yvert [a]

[a] Laboratoire d'Annecy-le-Vieux de Physique des Particules (LAPP), IN2P3/CNRS, Université de Savoie, Annecy-le-Vieux, France
[b] European Gravitational Observatory (EGO), Cascina (Pi), Italy
[c] INFN, Sezione di Firenze, Sesto Fiorentino, Italy
[d] Università Degli Studi di Firenze, Firenze, Italy
[e] Università Degli Studi di Urbino "Carlo Bo", Urbino, Italy
[f] LMA, Villeurbanne, Lyon, France
[g] INFN, Sezione di Napoli, Italy
[h] Università di Napoli "Federico II" Complesso Universitario di Monte S. Angelo, Italy
[i] Università di Salerno, Fisciano (Sa), Italy
[j] Departement Artemis – Observatoire de la Côte d'Azur, BP 4229 06304 Nice, Cedex 4, France
[k] LAL, Univ Paris-Sud, IN2P3/CNRS, Orsay, France
[l] ESPCI, Paris, France
[m] INFN, Sezione di Perugia, Italy
[n] Università di Perugia, Perugia, Italy
[o] INFN, Sezione di Pisa, Italy
[p] Università di Pisa, Pisa, Italy
[q] Università di Siena, Siena, Italy
[r] INFN, Sezione di Roma, Italy
[s] Università "La Sapienza", Roma, Italy
[t] National Institute for Subatomic Physics, NL-1009 DB Amsterdam, The Netherlands
[u] Vrije Universiteit, NL-1081 HV Amsterdam, The Netherlands
[v] INFN, Sezione di Roma Tor Vergata, Roma, Italy
[w] Università di Roma Tor Vergata, Roma, Italy
[x] Istituto di Fisica dello Spazio Interplanetario(IFSI), INAF, Italy
[y] Università dell'Aquila, L'Aquila, Italy
[z] AstroParticule et Cosmologie (APC), CNRS:UMR7164-IN2P3-Observatoire de Paris-Université Denis Diderot-Paris VII – CEA:DSM/IRFU, France
[aa] School of Physics and Astronomy, University of Birmingham, B15 2TT, UK

* Corresponding author.
  E-mail address: maddalena.mantovani@ego-gw.it (M. Mantovani).

ABSTRACT

During the past few years a network of large-scale laser interferometers, including the Virgo detector, has been developed with the aim of detecting gravitational waves. To properly operate the detectors, the longitudinal and angular positions of the suspended detector test masses, the interferometer mirrors, must be kept within a small range from the operating point.

The design of the Virgo angular control system, called Automatic Alignment is based on a modified version of the Anderson–Giordano technique, a wave-front sensing scheme which uses the modulation–demodulation technique.

This paper will present the theoretical background of the Virgo Automatic Alignment system, the implementation issues and the performances observed during the first Virgo science run (VSR1). A total RMS of 4×10^{-2} to 3×10^{-3} µrad for all angular degrees of freedom has been achieved.

Contents

1. Gravitational wave detection

Gravitational waves are one of the predictions of the *general theory of relativity* of A. Einstein; they are quadrupole emissions generated by the acceleration of masses which create perturbations of the space–time metric; up to now there has been no direct detection.

For this reason a set of interferometric gravitational wave detectors has been put into operation: Virgo [1] in Italy, LIGO [2] in the USA, GEO600 [3] in Germany, TAMA300 [4] in Japan and ACIGA in Australia [5]. These detectors are based on the Michelson interferometer topology, providing an unprecedented sensitivity with high duty cycle.

The detection principle of a large-scale gravitational wave interferometer is to sense the passage of a gravitational wave as a light intensity change at the asymmetric interference port due to the phase shift in the long arms. This is possible only if the test masses are suspended well enough to be considered as *free-falling test masses*.

Such instruments provide useful signal only when the optical components are positioned precisely at pre-defined locations relative to each other. This set of positions is called the *operating point*. Sophisticated electro-optical feed-back control systems are required to continuously measure and restore the mirror positions. Two separate systems to control the mirror position are used: one for the longitudinal position along the optical axis, and the other for the angular positions of the mirrors. Both of these control systems use a modulation–demodulation technique, at the same

modulation frequency, but in the first approximation, they can be decoupled since the longitudinal displacements have effects only on the TEM_{00} mode of the Gaussian beam, whereas the angular displacements affect the first higher order modes.

This paper will focus on the angular control system developed in the Virgo interferometer. After a brief introduction about the Virgo detector, the Automatic Alignment system will be described starting from the control principles, explaining the control technique by showing how the main interferometer beams are used to reduce the angular displacement of the mirrors, and showing the experimental improvements done in order to build a complete, robust angular control system for VSR1, the first Virgo scientific run (from May to October 2007). In the last part of the paper the performance of the angular control system is shown.

2. The Virgo detector

The Virgo interferometer is a ground based gravitational wave detector consisting of a Michelson interferometer with 3 km long Fabry–Perot cavities in its arms and a power recycling mirror [6]; see Fig. 1. The main optical elements are fused silica cylinders with a mass of 20 kg and diameter of 35 cm (except for the beam splitter mirror which is smaller). These are suspended in ultra-high vacuum by the so-called *super-attenuators* [7]. This suspension system provides an excellent seismic isolation in the range above the resonance frequencies of the mechanical system in the vertical and horizontal directions (more than 10 orders of magnitude above a
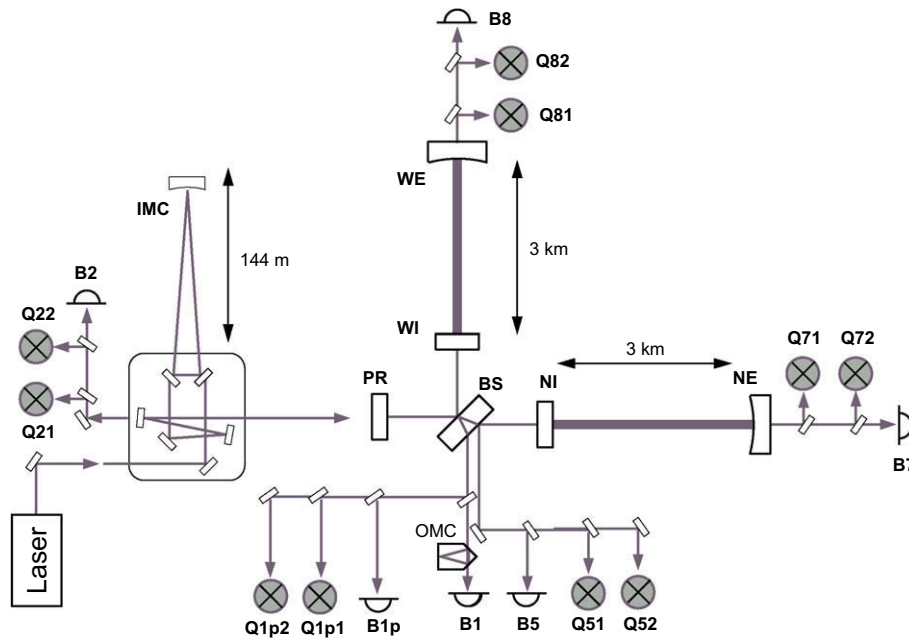
Fig. 1. Simplified scheme of the Virgo optical design. The diodes, placed on detection benches, used for longitudinal (with names starting with **B**) and angular (starting with **Q**) control system are shown. PR is the power recycling mirror, BS is the beam splitter, NI and NE are the input and end mirrors of the North cavity (equally for the West cavity), IMC and OMC are the input and output mode cleaners, respectively. See main text for details.
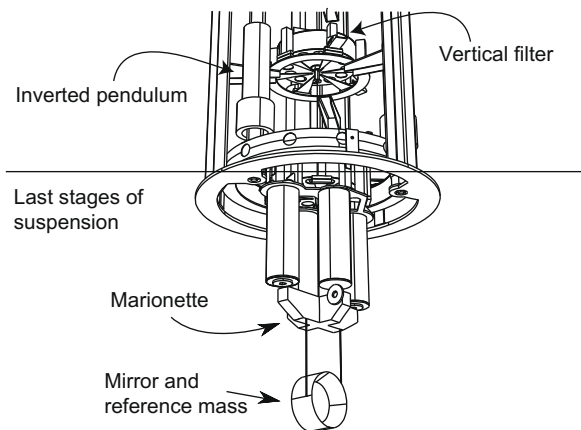

Fig. 2. Scheme of the last stage of the Super-attenuator suspension. The mirror is surrounded by a reference mass hanging from the marionette by means of steel wires. The seismic attenuation is obtained by the inverted pendulum, the vertical filters and the wires.

few Hz). The *super-attenuator* is composed of an inverted pendulum, with a very low mechanical resonant frequency, which provides a pre-isolation stage, and a cascade of attenuator filters.

The last stage of the suspension is formed by the *marionette* and the *reference mass*, see Fig. 2. The marionette, which is a massive element connected to the last vertical isolation stage, supports the reference mass and the mirror and acts on their position by means of four steel wires, in the longitudinal and in the angular degrees of freedom. The reference mass is a cylindrical like component which surrounds the mirror and acts on its position by coil-magnet actuators.

The input beam is generated by a system of master/slave lasers with a power of 20 W and a wavelength of 1064 nm. The beam jitter reduction is obtained by passing the input light through a 144 m long *input mode cleaner* (IMC), a triangular optical cavity. The laser beam is split at the *beam splitter* mirror (BS) into two

beams which are injected into the two orthogonal Fabry–Perot arm cavities (North and West arms), to enhance the phase shift produced by the optical path length variation of the beam.

The longitudinal position of all the mirrors is controlled in such a way that the arm cavities are on resonant and the recombination of the beams at the BS creates a destructive interference in the main output port (B1), called the asymmetric port, see Fig. 1.

This is the *dark fringe* condition. In this condition almost all the light power is reflected back to the power recycling mirror. The presence of this mirror allows to enhance the power circulating in the interferometer.

The light coming from the dark port of the interferometer is filtered by an *output mode cleaner* (OMC, a 2.5 cm monolithic cavity to reduce the higher order mode contents of the beam), before being detected by a set of high-sensitivity photo diodes at the B1 detection port.

3. The automatic alignment system

A misalignment or a displacement of a mirror produces a variation of the effective arm length of the interferometer which can mimic the effect of a gravitational wave. In order to reach the required strain sensitivity of Virgo, $h < 3 \times 10^{-21}/\sqrt{Hz}$ at 10 Hz, the position of the mirrors has to be actively maintained at the *operating point* with very high accuracy. Tolerable deviations from the operating point along the optical axis must be typically of the order of $\sim 10^{-15} - 10^{-12}$ m longitudinally [8] and $\sim 10^{-1} - 10^{-3}$ μrad of total RMS[1] for the angles, while the free motion of the suspended mirrors would be orders of magnitude larger than that; from 10 to 1 μrad see left plot of Fig. 3. The angular control system has to be implemented in order to reduce the mirror misalignments in the frequency region in which the super-attenuator does

---

[1] The angular accuracy can be roughly computed with the frequency domain simulation software Finesse [10] as the maximum angular misalignment of a given degree of freedom (d.o.f.) which does not spoil the required design contrast defect before the OMC, $C = 5 \times 10^{-4}$.
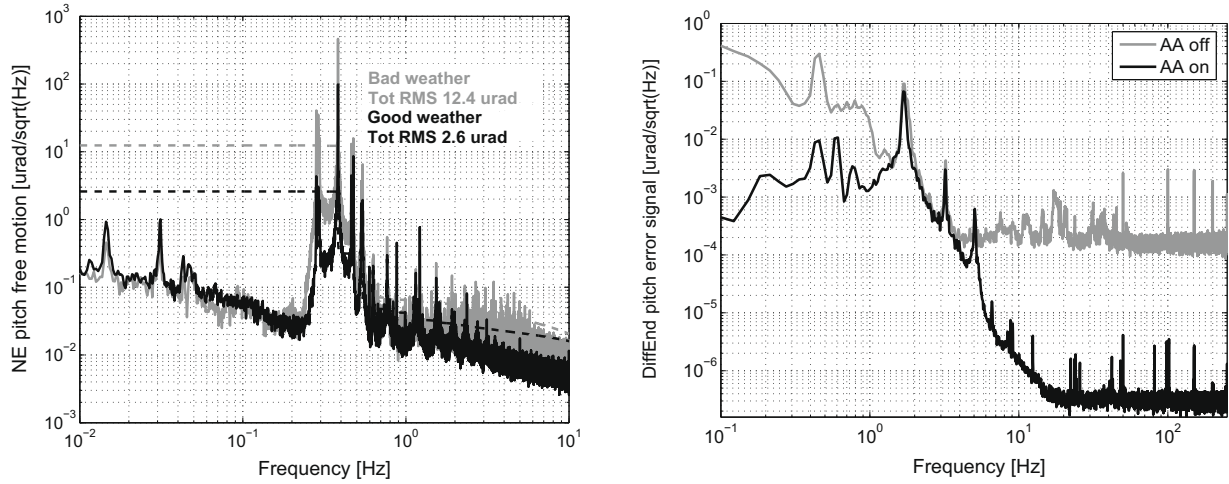
Fig. 3. *Left plot*: spectral comparison of the free motion of the NE pitch degree of freedom (d.o.f.) in case of bad and good weather conditions. The total RMS in both cases is well above the requirements and corresponds to ~2 µrad and to ~12 µrad for good and bad weather conditions, respectively. *Right plot*: spectral comparison between the Automatic Alignment error signal for the Differential End pitch d.o.f. under local control (AA off) and under global control (AA on). The high frequency noise is strongly reduced by switching from local to global control, reaching less than 10^{-5} µrad/$\sqrt{\text{Hz}}$ at 10 Hz due to the better performances of the global sensors.

not fulfill the alignment requirements, below the mechanical resonances (a few Hz).

During the engagement of the longitudinal control loops (called also *lock*), the angular positions of the main mirrors and of the beam splitter are controlled by using local references (called *local control* [11], with an accuracy of some µrad per hour).

The mirror angular positions in data taking mode cannot be controlled by the local controls due to the long term drifts of the references, which spoils the global overall alignment, and due to the high electronic noise of the sensors used, see right plot of Fig. 3.

After the lock has been acquired the angular control is switched to a global control system, the Automatic Alignment, which uses error signals coming from the interferometer itself.

The Automatic Alignment is a feed-back servo-loop system designed to reduce the fluctuations of the mirror angular positions with respect to the beam, thus maintaining the overall alignment of the optical elements and reducing the noise at the dark fringe port.

The aim of the Automatic Alignment system developed for the Virgo interferometer is to control the angular pitch and yaw[2] misalignments of the seven degrees of freedom, namely the PR, BS, NI, WI, Differential End $\left(\frac{\theta_{WE} - \theta_{NE}}{2}\right)$ and Common End $\left(\frac{\theta_{WE} + \theta_{NE}}{2}\right)$, and the main input beam (IB). The alignment error signals are extracted by using five beams coming out of the interferometer. They are: the main beam reflected by the interferometer (Q2), the two beams transmitted by the long arm cavities (Q7/8), the pick-off beam at the secondary surface of the BS (Q5) and the beam detected in the asymmetric port before the OMC (Q1p). At each detection port two quadrant diodes (*quadrants* for short) are installed, see Fig. 1.

As it is shown in the right plot of the Fig. 3 the local control electronic/shot noise is much higher than the noise of the global error signals. This electronic/shot noise starts to limit the global error signals from ~10 Hz, and its level is less than 10^{-4} µrad/$\sqrt{\text{Hz}}$.

4. The Anderson–Giordano technique for the angular control of Virgo

In order to properly control the angular degrees of freedom of the Virgo interferometer, a scheme for extracting angular error sig-

nals has been designed. The Automatic Alignment system is based on the Anderson–Giordano technique, a variant of the Anderson technique [12]. This is a modulation–demodulation method for alignment control based on differential wave-front sensing. The Anderson technique has been developed for the angular control of a single arm cavity. It uses an electro-optic phase modulator in the incident laser beam, and only one quadrant in transmission of the cavity to control the two cavity mirrors.

The quadrant is made of four sensitive elements, the sum over these four elements gives the same signal as a normal diode. Alignment control signals are obtained by demodulating at the modulation frequency the photo-current difference between the upper and lower elements for the pitch d.o.f., or the left and right for the yaw, at a common demodulation phase offset (ϕ_{dem}) obtaining the in-phase and in-quadrature signals.

The Anderson–Giordano technique is the extension for a full interferometer control. It uses two quadrants on each of five detection ports to have enough signals to decouple the various degrees of freedom to control in a complex system such as the Virgo optical system.

As it is shown in the Fig. 4 the error signals for the single cavity are detected in transmission by a set of two quadrants. The quadrants are placed, by means of telescopes, at a common Gouy phase offset (ϕ_{G}), and the Gouy phase difference between them is 90°.[3] It is required to have phase modulation of the input laser beam, with a modulation frequency which allows the first transverse Hermite–Gauss mode of the upper modulation sideband to be resonant in the arm cavities, in order to have a low noise error signal since it is amplified by the cavity gain. This resonance condition is fulfilled if the modulation frequency is:

$$f_{\text{mod}} = N \cdot \frac{c}{2L} + \frac{c}{2\pi L} \arccos \sqrt{1 - L/R_{\text{C}}} \tag{1}$$

where the first component of the second term is a multiple of the free spectral range of the cavity and the last component is the frequency separation between the fundamental and the first higher order mode; with N a positive integer, c is the speed of light, L the cavity length and R_{C} the terminal mirror radius of curvature [13].

---

[2] The pitch and yaw directions are defined as the rotation around the horizontal (x) and vertical (y)-axis, respectively, where the z axis is defined along the beam.

[3] The spatial distribution of a Gaussian beam depends on the longitudinal coordinate z which gives rise to an extra longitudinal phase lag with respect to the plane wave. The Gouy phase also determines the relative phases between the fundamental and higher order transverse Gaussian modes.
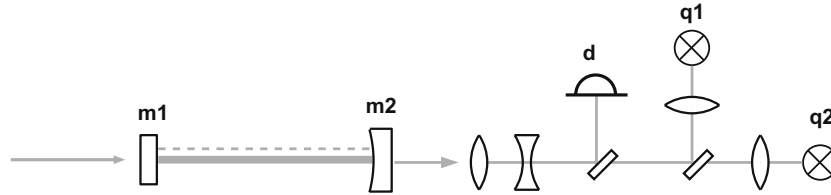
Fig. 4. Schematic of the optical layout of a single Fabry–Perot cavity designed for the Anderson–Giordano technique, in which the carrier fundamental mode (the continuous line) and the first higher order transverse mode of the upper sideband (the dashed line) are resonating. The alignment signals are detected in transmission of the cavity. Before the quadrants a telescope is used to set the common Gouy phase offset, while between the two quadrants the Gouy phase difference is fixed to be 90°.
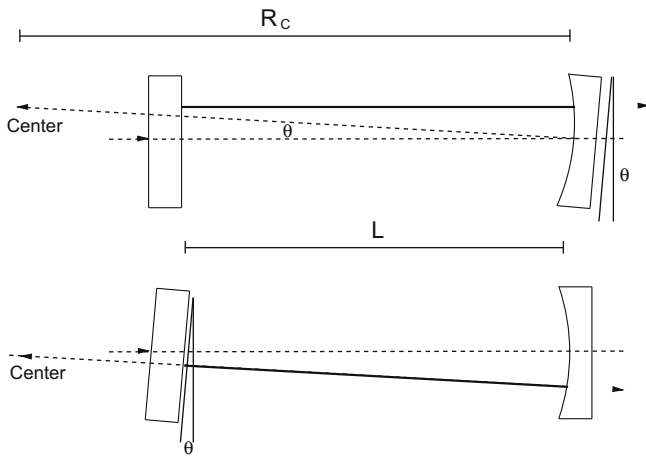

Fig. 5. Effect of misalignment of the two mirrors in a plane-concave cavity of length L for which the radius of curvature of the terminal mirror is R_C.

Considering also that the sidebands have to resonate in the IMC cavity and in the central interferometer, the small recycled Michelson interferometer composed of the PR, BS and the Input mirrors, and due to electronics constraints, the modulation frequency used in Virgo for longitudinal and angular control is $f_{mod} \sim 6.26$ MHz.

4.1. Single cavity example

The working principle of the Anderson–Giordano technique can be shown by using the single plano-concave cavity example, like the Virgo arm cavities. If the curved end mirror is misaligned by an angle θ, the cavity resonant mode will be purely translated by a quantity $R_C \cdot \sin(\theta)$; while if the flat input mirror is misaligned, a small translation, by $(R_C - L) \cdot \sin(\theta)$, plus a tilt, by θ, takes place, see Fig. 5. Thus a given misalignment can be defined as a combination of the *tilt* and *translation* eigenvectors of the resonant mode.

The error signals can be written then as [14]:

$$S1_I \propto \{\theta_{trans} \sin(\phi_G - \phi_{dem}) + \theta_{tilt} \cos(\phi_G - \phi_{dem})\}$$
$$S1_Q \propto \{\theta_{trans} \cos(\phi_G - \phi_{dem}) - \theta_{tilt} \sin(\phi_G - \phi_{dem})\} \tag{2}$$

where $S1_I$ and $S1_Q$ are the in-phase and in-quadrature error signal of the first quadrant (q_1), respectively. ϕ_G and ϕ_{dem} are the common Gouy and demodulation phase offsets and the θ_i are the normalized angles.[4] The error signals generated by the second quadrant diode can be easily computed by shifting the common Gouy phase offset ϕ_G of 90°.

Since the θ_{tilt} is generated exclusively by the misalignment of the input mirror and the θ_{trans} almost entirely by the misalignment

---

[4] The normalized angle mode corresponds to $\theta_{trans} = \frac{\Delta y}{\omega_0}$ for translation of the beam by Δy, and $\theta_{tilt} = \frac{\pi \theta \omega_0}{\lambda}$ for the tilt of the beam by an angle θ, where ω_0 is the beam waist and λ is the wavelength.

of the terminal mirror it is clear that it is possible to tune the common Gouy or demodulation phase offsets in order to perfectly decouple and control the two degrees of freedom. The Anderson–Giordano technique for the full interferometer control brings some advantages with respect the most used Ward technique [15], which uses the signals in reflection from the cavity, demodulated at a modulation frequency which does not enter in the cavity. For example the error signals detection in transmission which does not imply any wedges on the input mirrors for extracting the signals in reflection from the cavities. Moreover the possibility to decouple the angular degrees of freedom by tuning the demodulation phase with respect to the Gouy phases is a big advantage since it can be done remotely, without touching the telescopes, and the decoupling can be adjusted during all the phases of lock acquisition.

5. Automatic alignment control scheme

The control architecture becomes more complex for the global alignment of the whole recycled interferometer, due to the high number of degrees of freedom to control (7 per direction, pitch and yaw) which are strongly coupled due to the presence of the PR mirror, and the high number of error signals to deal with (10 quadrants which implies 20 RF signals, considering the in-phase and in-quadrature signal, and 10 DC asymmetry signals).

The control scheme is formed essentially by three parts: the error signal construction, by measuring the relation between the degrees of freedom to control and the quadrant signals (control matrix); the filtering, where the error signal is passed through control filters in order to construct the corrections; and the driving, where the corrections are distributed to the suspension actuators. The error and correction signals computation is managed by the global control system (GC) [17], which has the duty of gathering and processing any main interferometer output signals. The corrections are sent then to the suspension by DSP, digital signal processors, where also a common part of the local/global control filters are computed, in order to have a smooth transition in switching from local to global control.

5.1. Control matrix

The relation between the set of quadrant signals and the set of mirror tilts is expressed by the *optical matrix*. It represents the low frequency limit, below the cavity pole, of the transfer function between the angular degrees of freedom and quadrant signal [16], sampled at 500 Hz.

The optical matrix is measured by injecting sinusoidal excitations at the marionetta actuators, at low frequency from 0.1 Hz to 0.4 Hz in order to avoid the pendulum suppression above the mechanical resonance frequencies (a few Hz), and computing the transfer functions between the mirror angular positions and the quadrant signals at these frequencies. The control matrix is constructed by *inverting* the optical matrix. For an overdetermined

system the inversion of the optical matrix generates an infinite number of pseudo-inverse matrices, which are equivalent for the reconstruction of the degrees of freedom to control, but their properties differ for control noise issues. In order to reduce the control noise only the quadrant signals with strong signal to noise ratio have been considered.

5.2. Filtering and driving

The angular corrections are constructed by filtering the error signals with properly designed control filters. For the Automatic Alignment system two topologies of control have been developed: the *Fast control* and the *Drift control.*

The Fast control uses the global signals with a control bandwidth of a few Hz, where all the local controls are switched off.

The Drift control is a mixture of a global and local controls; the overall alignment is kept by a low frequency global control, with a few mHz of bandwidth, while the high frequency control is done by using local references, avoiding the slow independent drifts of the mirrors and maintaining a reasonably good global alignment.

In a perfectly decoupled control system all the angular degrees of freedom should be controlled by a fast control mode, but in reality strong couplings between the degrees of freedom to control are present. A way to separate them is to engage the controls with different control bandwidths: the dominant degrees of freedom should be engaged with a larger control bandwidth to reduce its impact on the other degrees of freedom.

Moreover the choice between fast and drift control depends also on noise issues. For example if a given d.o.f. has a strong coupling factor to the dark fringe it would be preferable to engage it with a fast control topology in order to have a larger control bandwidth, thus more accuracy, and a less noisy control (since the *local control system*, which has much higher electronic noise, is switched off); on the other hand if the error signal which senses that d.o.f. is noisy and the coupling factor into dark fringe is low it would be sufficient and advisable to engage that d.o.f. with a drift control since the narrow frequency band of the control helps in the decoupling of the d.o.f. from the dominant ones.

The design of the control filters for the fast control mode is a very important issue since the low frequency part, below the unitary gain frequency, determines the accuracy of the loop, and the high frequency part determines the noise performance of the loop. The control filter is developed starting from the modeling of the super-attenuator transfer function, from actuator to mirror, which is essentially a double pendulum with resonance frequencies at a few Hz. The control filters have to be designed in order to suppress the mechanical resonances of the suspension and to have a large low frequency gain.

The corrections are driven by means of the driving matrix inside the Gc which assigns to each suspension the right correction signal. The signals can be sent either to the marionetta or to the reference mass coil-magnet actuators.

In order to achieve good sensitivity performances in the first Virgo scientific run (VSR1), innovative features were applied to the Automatic Alignment system; such as reducing the re-injected control noise in the gravitational wave signal, by minimizing the angular coupling with the gravitational wave port signal, see Section 5.3, and adding a second modulation frequency to sense the Common End mirror mode, see Section 5.4.

5.3. Beam centering servo on the terminal mirrors

The noise performance of the angular control system in the detection band, above 10 Hz, is limited by the control noise re-injected into the mirrors. Due to the stability requirements of the control loop the roll-off of the control filter cannot be infinitely steep, thus the angular control noise will be introduced even in regions in which the free displacement of the mirror suspended to a super-attenuator is negligible.

The re-injection of control noise to the dark fringe signal is driven by several mechanisms. The direct mechanism of coupling between the angular noise and the gravitational wave signal is the coupling between the angular and longitudinal signals which is generated by the mis-centering of the beam on the mirrors.

The longitudinal coupling is directly proportional to the mis-centering of the beam on the mirror, as $\Delta L = y \cdot \sin(\theta)$, where y is the beam/mirror mis-centering and θ is the mirror misalignment. For this reason a part of the commissioning activity has been spent on the implementation of an automatic servo for *beam centering.* After the engagement of the alignment loops a sinusoidal excitation is applied to the terminal mirrors (with frequencies below the detection range, from 6 to 8 Hz). If the beam is not well centered on the mirrors, the sinusoidal excitation will be present also in the longitudinal error signals. The continuous centering servo applies a misalignment to the input mirrors in order to steer the beam on the terminal mirrors and minimize the angular/longitudinal coupling at the excitation frequency.

The beam/mirror centering is performed also on the other mirrors but only when it is considered to be necessary. The centering of the beam on the terminal mirrors has a strong effect on the dark fringe signal obtaining a noise coupling reduction up to some tens of Hz (above these frequencies the angular noise is well below the sensitivity) and a centering accuracy of about half a millimeter.

5.4. Additional modulation frequency

The alignment scheme of a large-scale interferometer is designed in order to fix the interferometer plane and then reduce the relative misalignment between the mirrors and the main beam. In the Virgo Automatic Alignment scheme the plane is defined by three points: the laser source and the beam pointing through the cavities. The beam is steered by aligning the input mirrors to strike the center of the terminal mirrors, see Section 5.3. All the other error signals should be only RF signals, in order to have real references for the alignment which do not depend on the relative position beam/quadrant.

Starting from the C6 commissioning run (July 2005 [16]), the alignment control scheme was active on all the main degrees of freedom, but with the use of the DC asymmetry of the Q21 quadrant (quadrant at the bright port) to control the Common End mode. The major problem is that this reference is noisy, since it is strongly affected by environmental noises, and not reliable, since it is affected by bench drifts and local excitations, while an RF signal would give an absolute reference (relative misalignment between the beam and the ITF).

In order to obtain a complete RF scheme investigations have been done,[5] it turned out that by using only one modulation frequency a complete RF scheme cannot be developed [18]. An additional modulation frequency, $f_{mod2} - 8.35$ MHz, which is completely reflected by the interferometer, can be used to evaluate the alignment deviation of the Common End mode in an absolute way. Essentially the quadrant in reflection of the PR mirror should detect the beat between the new modulation frequency sidebands and the reflection of the carrier which depends on the Common End mode displacement.

---

[5] A quality criterion for a designed control system has been developed, which is based on the capability of the sensing scheme to sense the angular position of the d.o.f. to be controlled [18]. The optical configuration is simulated by using the frequency domain simulation software *Finesse* [10], whose results are processed by Matlab scripts.

Since the implementation of the additional modulation frequency, February 2007, an improvement of the overall global alignment and of the repeatability of the lock was observed.

6. Performance

The angular control configuration for the Virgo detector was completed in the commissioning period between winter 2004 and the first scientific run; all the angular degrees of freedom were globally controlled, with a *fast* or *drift* control mode, depending on the noise performance of each loop, see Fig. 6. The quality of an angular control system can be evaluated by three factors: the robustness of the control against system perturbations; the accuracy of the control, which can be evaluated by the total RMS of the mirror angular displacements; and the noise performances, corresponding to the noise re-injected in the gravitational wave signal into the detection band (above 10 Hz).

6.1. Robustness

During the acquisition of the interferometer final state, the science mode, the angular control scheme passes through different phases. The first phase, called the *Cavity alignment*, is a pre-alignment phase of the interferometer arms. This is the least critical one: the cavity mirrors are controlled in a drift control mode with the PR mirror largely misaligned in order to prevent its reflected beam interfering with the light inside the interferometer.

When the PR is realigned, the optical system becomes completely different, due to the strong coupling between the degrees of freedom to control and the increase of circulating power which creates thermal effects due to mirror heating, such as the thermal transient [8]. In this phase the angular control is in the high noise configuration, in which smooth control filters with large gain/phase margins are used to survive the optical parameter evolution. In this phase the angular control loops are engaged one by one, and only the most critical d.o.f. control loops are activated, such as the Differential End and the PR controls.

When the thermal transient phase is finished the less critical degrees of freedom, such as the input mirrors, are then controlled. This is the final state in which more optimized control filters are used, with high gain at low frequencies in order to ensure a good accuracy and low high frequency gain in order to not spoil the sensitivity in the detection band by re-introducing control noise.

The control system allowed a continuous lock of the interferometer in VSR1 of more than 94 h with a high duty cycle of scientific data taking of ∼81%. The losses of science mode lock due to alignment control failures were ∼2%, mostly due to electronics equipment failures.

6.2. Accuracy of the automatic alignment control loops

The accuracy of an alignment feed-back control loop can be evaluated by measuring the residual RMS of the calibrated error signals and it mainly depends on the low frequency gain of the control, see Fig. 7. The requested accuracy of the control depends on the coupling factor between the d.o.f. and the gravitational wave signal. The degrees of freedom which have a larger coupling factor into the dark fringe are the ones which have a differential effect on the optical paths in the cavities, such as the Differential End mode.

From the Table 1 it can be noticed that these critical degrees of freedom are controlled in such a way that the residual angular motion is of the order of 10^{-3} μrad, while a less stringent control is applied to the angular degrees of freedom which have a smaller coupling factor, such as the Common End modes. It can be noticed also that the accuracy of some of the d.o.f. to control do not fulfill the requirements. It is due mostly to the low frequency
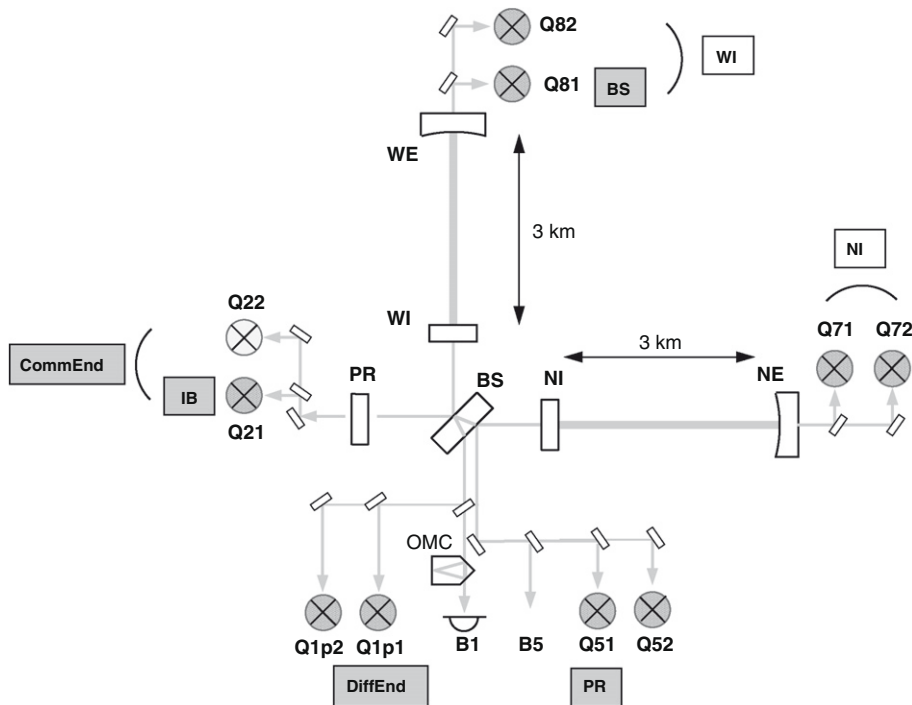

Fig. 6. Configuration of the automatic alignment control scheme for the science run VSR1. The Q22 quadrant (light grey) has been demodulated at the additional modulation frequency (∼8.35 MHz), described in Section 5.2. The schematic shows the signals used to control each d.o.f. (labeled in a grey or white box). The degrees of freedom labeled in grey are controlled by using a fast control topology while the white ones are controlled in drift control mode. For example the differential end mode is controlled by using the Q1p1 quadrant signal in fast control mode (for the differential end mode the error signal is extracted at the asymmetric port before the OMC in order to not suppress the higher order modes content).
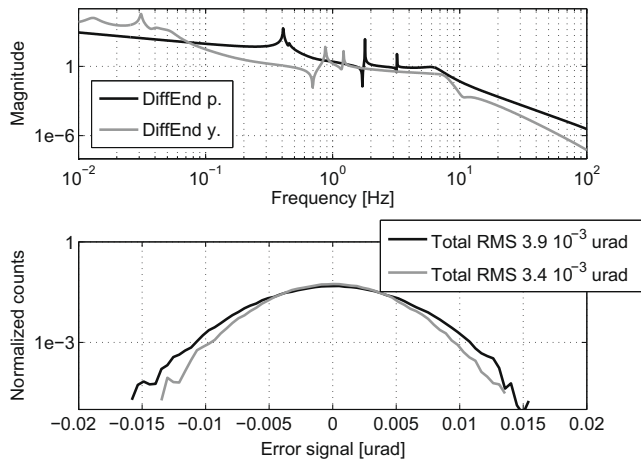
Fig. 7. The top plot shows the control filters for the differential end pitch and yaw degree of freedom. The control filters are designed in order to compensate the mechanics of the super-attenuator providing a large low frequency gain, to ensure a good accuracy, and to have a strong roll-off to do not re-inject control noise in the detection band. The bottom plot shows the accuracy of the error signals, evaluated by the total RMS of the distribution. We can notice that the differential end yaw d.o.f. has larger very low frequency gain which ensures a better accuracy in the control.

Table 1
Accuracy of the angular control loops expressed in total RMS. The accuracy is between 4×10^{-2} and 3×10^{-3} µrad.

D.o.f. accuracy	Pitch Total RMS (µrad)	Yaw Total RMS (µrad)	Design Total RMS (µrad)
PR	8×10^{-3}	1.3×10^{-2}	1×10^{-2}
BS	3.3×10^{-2}	3.4×10^{-2}	
Diff. end	4×10^{-3}	3×10^{-3}	3×10^{-3}
Comm. end	3.3×10^{-2}	4.3×10^{-2}	2×10^{-2}

environmental noise due to slow air fluxes on the detection benches which effect the error signals in the region between ~100 mHz and a few Hz. In order to improve the accuracy of the control plexiglas covers will be installed on the most critical detection benches to reduce the air fluxes.

6.3. Noise performance

The noise performance can be defined as the effect of the Automatic Alignment system to the detector sensitivity in the detection band, starting from 10 Hz. Since the unity gain frequency of the angular controls is of the order of a few Hz the noise performance depends on the dark fringe coupling factor, on the high frequency performances of the control filters and on the high frequency sensor noise (electronic plus shot noise).

In order to evaluate the effect of the Automatic Alignment control noise on the sensitivity a direct measurement of the noise budget has been made. A coloured noise is injected at the error signal level to measure the transfer function between the angular displacement and the gravitational wave signal in the detection band [20]. This transfer function is then applied to the control signals to estimate how much control noise is present in the dark fringe.

The Fig. 8 shows the angular noise budget obtained in March 2008. The total control noise is below the measured Virgo sensitivity curve, and above 20 Hz it is below the design sensitivity.

Design sensitivity, starting from 10 Hz, for the angular control noise can be achieved by using improved electronics and by improving the control filters cut-off design. All the sensing electronics for the angular control will be replaced in the Virgo+ commissioning period (form November 2008), which will allow the detection of larger powers, up to 30 mW, and to have lower electronic/shot noise (better by a factor ~3); moreover the Global control system will be upgraded allowing the use of more complex and high performance control filters.

7. Conclusions

A complete and functioning Automatic Alignment control system was developed and refined between winter 2004 and May 2007. The coupling between the angular and longitudinal signals has been reduced by applying a continuous centering servo to better center the beam on the End mirrors. The robustness has been improved by designing proper control filters for the angular control for each phase of the lock acquisition up to the science mode. Only ~2% of the losses of lock in science mode were due to the alignment control system.

The noise performance has been optimized to have a control noise well below the best measured Virgo sensitivity, for any
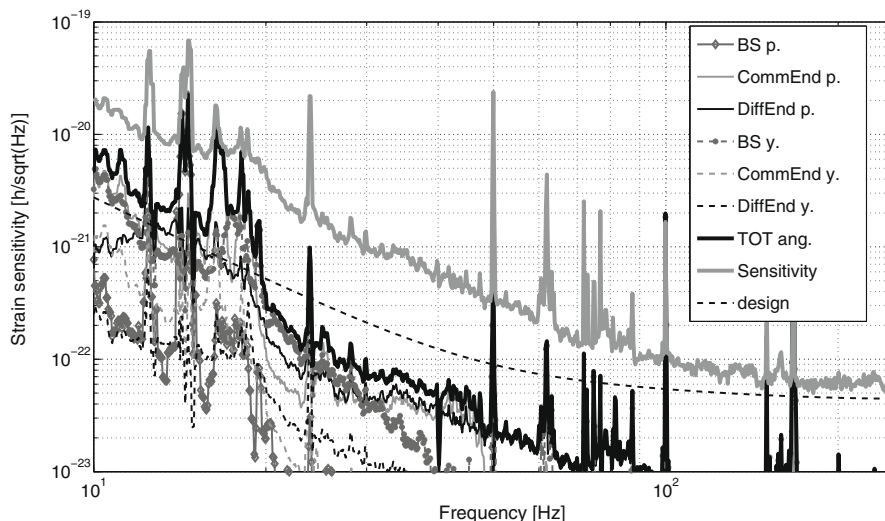

Fig. 8. Noise budget of the automatic alignment control system in March 2008 compared to the design sensitivity curve and to the measured sensitivity. The total angular noise is well below the sensitivity curve and below the Virgo design above 20 Hz. The peaks in the region between 10 and 20 Hz are mainly due to environmental noises.

frequency range in the detection band, and below the design sensitivity above 20 Hz.

The system is still under improvement in order to fulfil the requirements for Virgo and Virgo+, where a larger input power will be used and a monolithic mirror suspension will be eventually installed. The improvements include the upgrade of the sensing electronics; the normalization of the error signal, with the input power, in order to increase the robustness of the system during all the lock acquisition phases; the increase of the alignment error signals sampling frequency to 1 kHz, to reduce the control time delay; and the reduction of environmental noise which couples with the angular error signals.

References

[1] F. Acernese, et al., Status of Virgo, in: Proceedings of the Seventh Amaldi Conference, Sidney, 2007.

[2] D. Sigg, et al., Status of LIGO detectors, in: Proceedings of the Seventh Amaldi Conference, Sidney, 2007.

[3] H. Grote, et al., Status of GEO 600, in: Proceedings of the Seventh Amaldi Conference, Sidney, 2007.

[4] R. Takahashi, et al., Operational status of TAMA300 with the seismic attenuation system (SAS), in: Proceedings of the Seventh Amaldi Conference, Sidney, 2007.

[5] D.E. McClelland et al., Second-generation laser interferometry for gravitational wave detection: ACIGA progress, Class. Quant. Grav. 18 (2001) 4121–4126.

[6] J.Y. Vinet et al., Optimization of long baseline optical interferometers for gravitational wave detection, Phys. Rev. D 38 (1988) 433–447.

[7] G. Ballardin et al., Virgo Collaboration, Rev. Sci. Instr. 72 (9) (2001) 3643–3652.

[8] F. Acernese et al., Virgo Collaboration, lock acquisition of the Virgo gravitational wave detector 31 (1) (2008) 29–38.

[10] A. Freise, G. Heinzel, H. Luck, R. Schilling, B. Willke, K. Danzmann, Frequency domain interferometer simulation with higher order spatial modes, Class. Quant. Grav. 21 (2004) S1067.

[11] F. Acernese et al., Virgo Collaboration, A local control system for the test masses of the VIRGO gravitational wave detector, Astrop. Phys. 20 (2004) 617–628.

[12] D.Z. Anderson, Alignment of resonant optical cavities, Appl. Opt. 23 (1984) 2944–2949.

[13] F. Acernese, et al., VIRGO Collaboration, Automatic mirror alignment for VIRGO: first experimental demonstration of the Anderson technique on a large-scale interferometer, arXiv:gr-qc/0411116.

[14] M. Mantovani, The automatic alignment in the Virgo interferometer, Ph.D. Thesis for the Università Degli Studi di Siena.

[15] E. Morrison, Appl. Opt. 33 (1994) 504.

[16] F. Acernese et al., Virgo Collaboration, The Virgo automatic alignment system, Class. Quant. Grav. 23 (2006) S91–S102.

[17] F. Cavalier et al., Virgo Collaboration, The global control of the Virgo experiment, Nucl. Instr. Meth. Phys. Res. 550 (2005) 467–489.

[18] M. Mantovani, A. Freise, Evaluation of alignment sensing matrices using row vector orientation, in: Proceedings of the Seventh Amaldi Conference, Sidney, 2007; Journal of Physics: Conference Series 122 (2008) 012026.

[20] G. Vajente, Analysis of sensitivity and noise sources for the Virgo gravitational wave interferometer, Universita' di Pisa, Ph.D. Thesis, 2008.